RSC Advances

PAPER

View Article Online
View Journal | View Issue

Cite this: *RSC Adv.*, 2023, **13**, 6396

Fabrication and characterization of a flexible and disposable impedance-type humidity sensor based on polyaniline (PAni)†

D. Yureka Imali, * E. Chavin J. Perera, M. N. Kaumal and Dhammike P. Dissanayake

This work presents a highly sensitive, economical, flexible, and disposable humidity sensor developed with a facile fabrication process. The sensor was fabricated on cellulose paper using polyemaraldine salt, a form of polyaniline (PAni), *via* the drop coating method. A three-electrode configuration was employed to ensure high accuracy and precision. The PAni film was characterized using various techniques including ultraviolet-visible (UV-vis) absorption spectroscopy, Fourier transform infrared spectroscopy (FTIR), X-ray diffraction (XRD) and scanning electron microscopy (SEM). The humidity sensing properties were evaluated through electrochemical impedance spectroscopy (EIS) in a controlled environment. The sensor exhibits a linear response with $R^2 = 0.990$ for impedance over a wide range of (0%–97%) relative humidity (RH). Further, it displayed consistent responsiveness, a sensitivity of 1.1701 Ω/%RH, acceptable response (≤220 s)/recovery (≤150 s), excellent repeatability, low hysteresis (≤2.1%) and long-term stability at room temperature. The temperature dependence of the sensing material was also studied. Due to its unique features, cellulose paper was found to be an effective alternative to conventional sensor substrates according to several factors including compatibility with the PAni layer, flexibility and low cost. These unique characteristics make this sensor a promising option for use in specific healthcare monitoring, research activities, and industrial settings as a flexible and disposable humidity measurement tool.

Received 1st January 2023
Accepted 14th February 2023

DOI: 10.1039/d3ra00009e

rsc.li/rsc-advances

1. Introduction

Researchers and scientists have conducted numerous experimental works to investigate humidity sensors with better response/recovery, high sensitivity, ease of fabrication, stability and efficiency.[1,2] Humidity is a critical factor in fields such as manufacturing and storage processes in industries, agriculture, climatology, medical and domestic applications.[3–8] Therefore, various types of humidity sensors have been developed using different fabrication technologies, sensing materials and sensing mechanisms.[3,9] Among these humidity sensors, the sensors that are made using conducting polymers as sensing material (organic polymer type) are very special due to easy preparation, low fabrication cost, high sensitivity and short response time.[10,11]

These types of polymers are referred to as intrinsically conducting or electroactive conjugated polymers. Conducting polymers have a π-electron backbone, which accounts for their electronic properties. These structural characteristics caused to have special properties in conducting polymers such as electrical conductivity, low energy optical transitions, low ionization potentials and high electron affinity.[12,13]

Organic polymer-type humidity sensors consist of an electrode pair on an insulating substrate and a layer of the polymer film in contact with electrodes.[10,14] When water molecules are absorbed by the upper layer of sensing material/conducting polymer, resistivity between electrodes changes and it can be measured using an electronic circuit/device as a physical signal such as conductivity, impedance and current of the sensor.[10,15] As a result of the interaction between the water molecules and the nitrogen centers of the polymer backbone, hydrogen bond formation occurs. This process increases the conductivity of the material.[8]

In these organic polymer-type humidity sensors conducting polymers with hydrophilic properties are used as the sensing material.[4] PAni is one of the conducting polymers used in humidity sensors. It is a polymer characterized with high stability, ease of fabrication, acid–base properties and redox activity.[6,13,16,17] PAni is a mixed oxidation state polymer.[18] It has three different oxidation states.[19] These are leucoemeraldine, emeraldine and pernigraniline. This classification is done based on the amine to imine ratio. Among these three states, the fully reduced state is leucoemeraldine which is the PAni chain consisting of linked imine. The fully oxidized state is pernigraniline and it contains amine. The emeraldine form is neutral (amine : imine ratio ≈ 0.5) and due to possessing

Department of Chemistry, University of Colombo, Colombo 03, Sri Lanka. E-mail: yurekauoc@gmail.com

† Electronic supplementary information (ESI) available. See DOI: https://doi.org/10.1039/d3ra00009e

electrical conductivity and high stability at room temperature, it is considered as the most useful form of PAni while the other two forms are electrically insulating.[20,21] The basis of the water sensitivity of PAni is the existence of oxidation states.[6]

Previous researchers have conducted studies on utilizing PAni in humidity sensor fabrication. Kulkarni *et al.* employed PAni to develop a flexible humidity sensor with inkjet print technology which involved the synthesis of aqueous, PAni-based ink.[22] Liu *et al.* developed a humidity sensor using PAni nanofibers.[23] Machappa *et al.* developed a humidity sensor with PAni and the inclusion of tungsten disulfide facilitated the absorption of water molecules by augmenting the porous structure.[24] Chani *et al.* also reported a humidity sensor fabricated with PAni thin films on a glass substrate, exhibiting a more uniform correlation between humidity and impedance in comparison to capacitance.[6]

Majority of the humidity sensors require complex and costly fabrication methods.[6] In contrast, this current work developed a cost-effective sensor that requires miniscule quantities of chemicals and paper as the sensor substrate. Moreover, a simple technique was used for the fabrication process. Some applications require flexible humidity sensors, to be used in applications such as skin-like electronics, wearable electronic systems and robotic human–machine interfaces[25] while some other applications require low-cost, disposable humidity sensors for one-time usability. The detection of body moisture/gathering body health information in biomedical applications and extreme research activities involving toxic substances including biological and chemical warfare agent analysis are some examples. However, the compatibility of this sensor in extreme environments is yet to be analyzed. Therefore, this study focuses on finding a solution to the above issues by developing an organic polymer-type humidity sensor using cellulose paper as the sensor substrate for particularly use where disposable and flexible humidity sensors are required. The sensor repeatability, reversibility, hysteresis, long-term stability, response–recovery time, and effects of temperature, ethanol vapor and CO_2 were investigated. Further, the effect of sensor substrate for functionality of the sensor was studied. Scanning electron microscopy (SEM) was used to examine the morphology of the PAni film. X-ray diffraction (XRD), Fourier transform infrared (FT-IR) spectroscopy and ultraviolet-visible (UV-vis) absorption spectroscopy were used to determine the semicrystalline microstructure, chemical structure and oxidation state of the synthesized PAni.

2. Experimental

2.1 Reagents and materials

All the reagents used were prepared from analytical grade chemicals and all solutions were prepared in distilled water. Aniline (≥99.5%, Sigma Aldrich), sulphuric acid (≥98%, Sigma Aldrich) and potassium persulfate (≥99%, Fluka) were used for PAni synthesis.

Whatman® cellulose chromatography paper (material-cellulose membrane sheets) was used for paper-based sensor and transparent polyester (PET) film was used for transparent sheet-based sensor. Graphite powder (200 μm) obtained from Kahatagaha Graphite Lanka, Sri Lanka and commercially available varnish were used to fabricate carbon electrodes. Silver conductive ink (CircuitWorks® Silver Conductive Pens) was used to fabricate the reference electrode.

$CaCl_2$ anhydrous, granular (≥93.0%, Merck), LiCl (≥99.98%, Sigma Aldrich), $MgCl_2$ (≥98%, Sigma Aldrich), K_2CO_3 (≥99.0%, Merck), $Mg(NO_3)_2 \cdot 6H_2O$ (≥99.99%, Sigma Aldrich), NaCl (≥99.5%, Sigma Aldrich), KCl (≥99.0%, Sigma Aldrich), KNO_3 (≥99.0%, Sigma Aldrich), K_2SO_4 (≥99.0%, Fluka) were used to prepare saturated salt solutions.

2.2 Instrumentation

An oven (Memmert, Germany) capable of maintaining temperature of 105 ± 5 °C was used to anneal the sensor. A portable conductivity meter (WPA model CM35) was used to take conductance measurements of the sensor at different humidity environments. A multimeter (Sanwa – cd800a, Japan) was used to measure resistance of carbon electrodes. Electrochemical impedance spectroscopy (EIS) studies were performed using ZIVE SP5 workstation (WonTech, Korea). PAni characterization was done using UV-vis spectrophotometer (Thermo Scientific – GENESYS 180), FT-IR spectrophotometer (PerkinElmer – Spectrum Two), Scanning Electron Microscope (Zeiss evo 1s 15), X-ray powder diffractometer (Rigaku SmartLab).

2.3 Fabrication of the sensor

Graphite powder and varnish (1 : 1) thick paste was used to fabricate two carbon electrodes on the chromatography paper. Aniline (0.1 M) solution was prepared and it was acidified with few drops of H_2SO_4 acid. $K_2S_2O_8$ (0.1 M) solution was prepared as the chemical oxidant. An equal amount of monomer and the oxidant were added dropwise on to the chromatography paper strip which has pre-deposited carbon electrodes and allowed polymerization to take place. This process was continued several times within 30 minutes intervals until the green coloured emeraldine form of PAni was formed. After keeping fabricated sensor at room temperature for few hours to dry, the sensor was annealed at 100 °C in an oven for 1 hour. Silver conductive ink was used to fabricate the pseudo reference electrode.

2.4 Characterization of PAni film

2.4.1 Ultraviolet-visible spectroscopy. The oxidation state of synthesised PAni film was determined using UV-vis absorption spectroscopy. PAni film was deposited on a quartz slide, applying the same conditions as in sensor preparation. Then the UV-vis absorption spectrum was collected in the wavelength range of 260–1000 nm at room temperature.

2.4.2 FTIR spectroscopic measurements. The Attenuated Total Reflection Fourier transform infrared (ATR FTIR) spectra of chromatography paper, sensor equilibrated at 0%, 75% and 97% RH levels were recorded. The wavelength range of the spectra was 600–3800 cm^{-1}.

2.4.3 Scanning electron microscopy characterization. PAni film morphology was studied using Scanning electron microscope. Scanning electron micrograph was obtained at an accelerating voltage of 20 kV. The PAni film was gold sputtered before SEM analysis.

2.4.4 XRD characterization. XRD analysis was carried out using Cu Kα radiation ($\lambda = 0.154$ nm) over a 2θ range of 10–70° with a step size of 0.02° and a step time of 1 s.

2.5 Evaluation of humidity sensing performances

EIS and conductivity studies of the sensor were performed by keeping the sensor in humidity-controlled chambers at room temperature (30 °C). Saturated salt solutions were used to generate the controlled humidity environments. In controlled humidity systems, a saturated salt solution is equilibrated with water vapor to get the required water vapor pressure.[26,27] The humidity series consisted of nine humidity chambers with nine different relative humidity (RH) levels. Every humidity chamber contains a different saturated salt solution as well as a vapor phase that has a specific RH value. Humidity chambers were prepared in identical glass bottles with airtight caps. The nine saturated salt solutions used in the series and their corresponding RH values are dry $CaCl_2$ (0%), LiCl (11%), $MgCl_2$ (32%), K_2CO_3 (43%), $Mg(NO_3)_2$ (51%), NaCl (75%), KCl (84%), KNO_3 (92%), K_2SO_4 (97%).[26–29]

2.5.1 Conductivity measurements of the sensor. The conductivity of the sensor at nine different RH levels were measured using a portable conductivity meter. Prior to take measurements, the sensor was kept at the particular RH level allowing it to reach the equilibrium between sensor surface and water vapor.

2.5.2 Measurement of electrochemical impedances. EIS responses for entire humidity series were collected keeping the sensor at each RH level in the frequency range of 1 Hz to 1 MHz, with amplitude potential of 10 mV. The electrochemical impedance spectra were collected under 0 V biased potential against the pseudo-reference electrode.

2.5.3 Temperature effect on the sensor. Electrochemical impedance spectra at room temperature were collected in the presence and absence of N_2 gas. Further, electrochemical impedance spectra at 40 °C, 50 °C, 60 °C, 70 °C, 80 °C, 90 °C, 100 °C, 110 °C, 120 °C, 130 °C and 135 °C were obtained after flowing a constant flow of N_2 gas through the sensor chamber for 15 minutes.

2.5.4 Determination of humidity sensing parameters. The selectivity of the sensor was studied against ethanol vapor (a polar interfering VOCs gas) and CO_2 (an inorganic interfering gas). Electrochemical impedance spectra were collected at different RH levels in the presence and absence of these gases and responses were compared. A test tube with a few drops of absolute ethanol was placed inside the humidity chamber to produce ethanol vapor and CO_2 gas was evolved within humidity chambers by reacting $CaCO_3$ and HCl. Long term stability of the sensor was studied measuring impedance of the sensor at 0%, 75% and 97% RH levels once every 5 days throughout one-month period.

3. Results and discussion

3.1 Structural characteristics

3.1.1 Chemical structure of PAni film. The presence of conducting state of PAni, the polyemaraldine salt can be detected using absorption spectroscopy.[30] The UV-vis absorption spectrum of PAni film is shown in Fig. 1. Three characteristic peaks can be observed in the absorption spectrum: ~350 nm, ~416 nm, and ~838 nm. The π–π* electron transition of benzenoid rings was represented by the absorption peak at ~350 nm.[30–32] The absorption peaks observed in the visible region at ~416 nm and ~838 nm correspond to the polaron state transitions assigned to π-polaron and polaron-π*, respectively.[30,32] These two peaks indicate the presence of conductive salt form of PAni.[30]

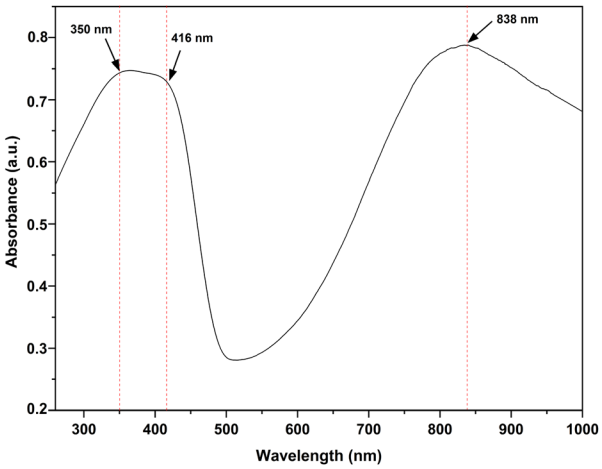

Fig. 1 UV-vis absorption spectrum of PAni film.

The PAni film was spectroscopically characterized using FTIR. The FTIR analysis of chromatography paper and paper-based PAni humidity sensor at 0%, 75% and 97% RH levels were conducted to identify changes that occur due to water vapor absorption. Fig. 2 shows the FTIR spectrums of PAni film at RH 0%, RH 75% and RH 97% within 600–1700 cm^{-1} which contains the characteristic bands of PAni. The peaks that appeared at around 1568 cm^{-1} and 1482 cm^{-1} correspond to C=C stretching vibrations of quinoid and benzenoid rings,

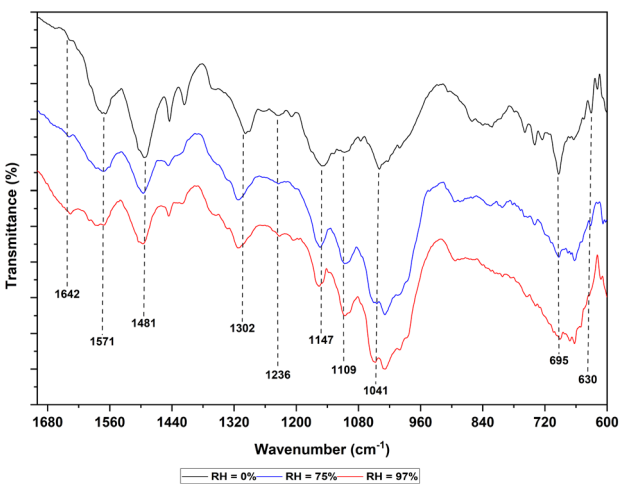

Fig. 2 FTIR spectrums of PAni film at RH 0%, RH 75% and RH 97%.

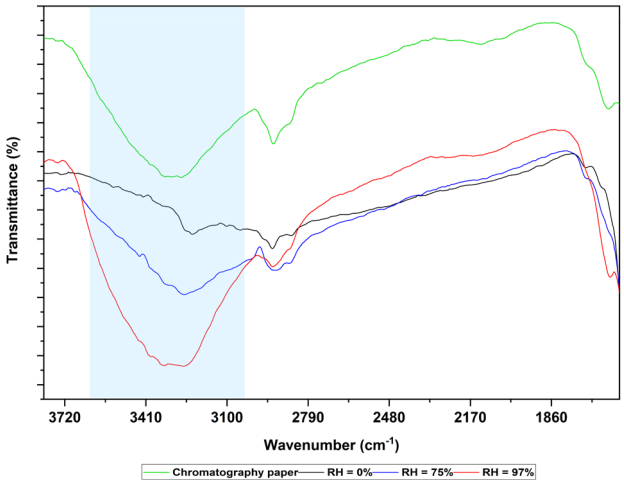

Fig. 3 FTIR spectrums of chromatography paper and PAni film at RH 0%, RH 75%, RH 97% (from 3750 cm^{-1} to 1700 cm^{-1}).

respectively. The peak around 1300 cm^{-1} corresponds to the C–N stretching vibrations.[13,33–36]

The aromatic C–H in-plane vibrations are usually observed in the region of 1010–1170 cm^{-1} as well as C–H out-of-plane vibrations are recorded in the region of 800–880 cm^{-1}.[33,36] The peak observed at around 1232 cm^{-1} corresponds to the C–N^{+} stretching vibrations in the polaron structure which is characteristic of the emaraldine salt, the conducting protonated form of PAni. The 1147 cm^{-1} band is assigned to –NH^{+}= stretching vibrations.[33] The formation of –NH^{+}= groups occurs as a result of protonation. This reveals the extent of electron delocalization as well as the characteristics of its electrical conductivity. The peak observed at 695 cm^{-1} corresponds to the S–O stretching vibrations and the peak at 630 cm^{-1} is for the C–S stretching-vibrations.[33] These modifications are associated with the product transformation from pernigraniline to emeraldine due to protonation by sulphuric acid.[37]

Fig. 3 shows the FTIR spectrums of PAni film at RH 0%, RH 75%, RH 97% and chromatography paper in 1600–3800 cm^{-1} range. As shown in Fig. 3, when the sensor was exposed to water vapor, characteristic broad peak of water appeared around 3271 cm^{-1}.[27] It can also be observed that the peak area of these peaks increased as humidity increased. This observation can be attributed to the increase of absorbed water molecule concentration in PAni film with increasing humidity. Another distinctive water peak appeared 1642 cm^{-1}.[27] The broad peak observed in the IR spectrum of chromatography paper at 3272 cm^{-1} corresponds to the OH groups present in the cellulose structure.[38] FTIR and UV-vis spectra confirmed that the chemical structure of the PAni film is conductive polyemaraldine salt.

3.1.2 Morphology. PAni film deposited on paper was analysed and surface morphologically characterized by SEM. The SEM picture of PAni film with low and high magnifications are shown in Fig. 4(a) and (b), respectively. The synthesis conditions influence the PAni morphology.[39] For example, the acidity conditions during the reaction have the following effects on the

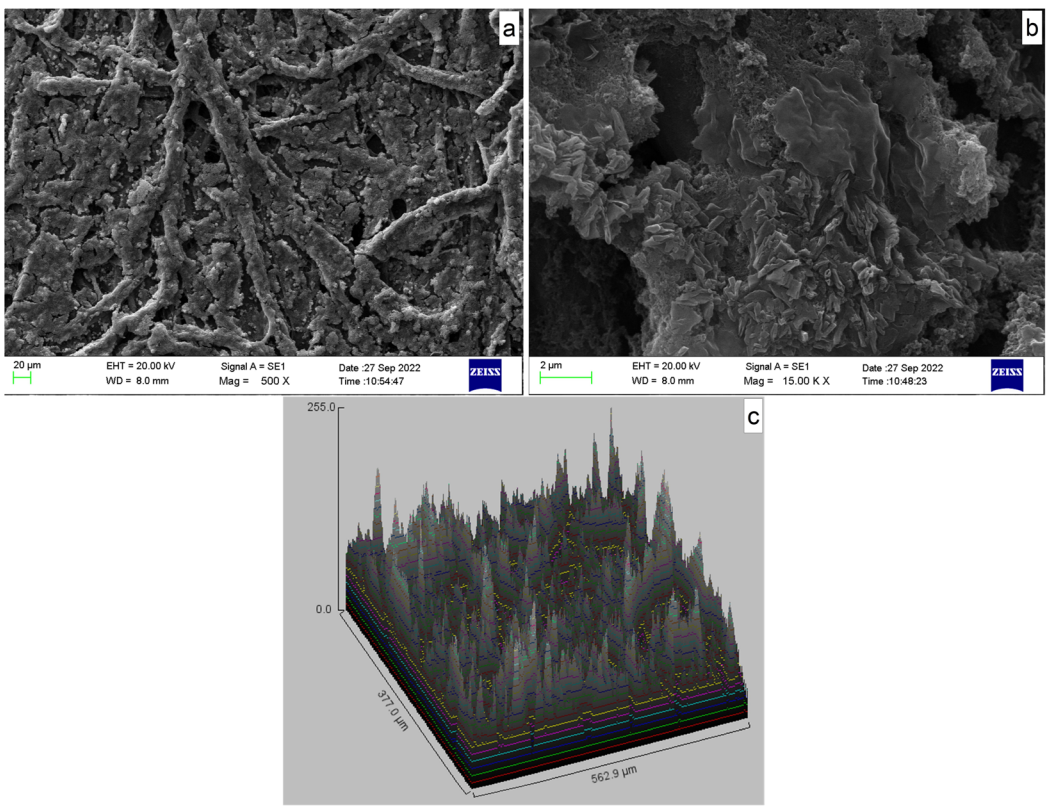

Fig. 4 SEM images of the PAni film (a) low magnification (500×), (b) high magnification (15.00 KX) and (c) surface roughness.

morphology of PAni. The granular PAni was produced with sulfuric acid.[37] Precipitation polymerization followed by strong oxidants and high aniline concentrations under strongly-acidic conditions (at pH < 2) generates PAni with granular morphology.[39] The distinct characteristics which are consistent with the morphology of pure PAni are the existence of globular clusters, weak linkages between PAni chains, and relatively high porosity.[13] SEM micrograph of chemically polymerized PAni film of paper-based humidity sensor as in Fig. 4(a) with low magnification, shows a branched root like structures over micro granule aggregates. These branched root-like structures are supposed to increase the movement of charge carriers resulting in high conductivity. In high magnification, coral-like morphology can be observed (Fig. 4(b)). This has resulted in highly porous nature with a large amount of void space throughout the film. This porous nature of the PAni film is significant in its humidity sensing process as these micropores increase water adsorption by increasing surface area and providing more adsorption sites and improving the film's humidity sensing properties.[24,34] As some areas are denser than others, an uneven distribution of PAni layer can be identified. Therefore, the surface morphology of PAni layer is non-uniform and heterogenous. Fig. 4(c) shows the detailed 3D surface plot of the PAni film over a surface area of 377.0 × 562.9 μm^2. Surface roughness enhances the gas permeation rate of membranes.[40] The roughness parameter R_a (average roughness) is used to assess the surface roughness and computed along with ImageJ software (roughness calculation plugin). For the PAni layer, the R_a value is 16.9 μm which is considerably higher than the past literature values recorded with respect to different type of PAni films.[41–43]

3.1.3 Semicrystalline microstructure. The degree of crystallinity of PAni was determined using XRD. PAni is a two-phase system and semi-crystalline in nature. Polymer chains in the crystallites phase are parallel and closely packed, whereas they are not parallel or ordered in the amorphous phase.[39] The obtained XRD pattern of PAni film is shown in Fig. 5. Two wide peaks were found at $2\theta = 20°$ and 25°. The peak observed at $2\theta =$ 25° is the characteristic peak of the PAni salt and it indicates the semicrystalline structure of PAni film. The crystalline structure is due to the benzenoid and quinoid rings in PAni chains.[44] The crystallinity is beneficial for the rapid transportation of charge carriers from the PAni film surface to the bulk.[45]

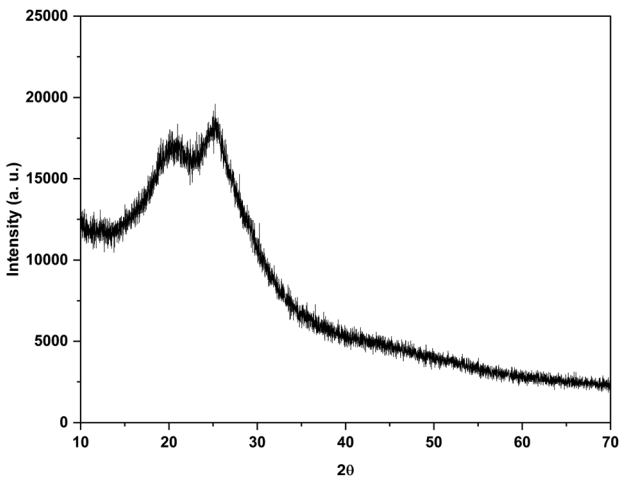

Fig. 5 XRD pattern of synthesized PAni.

3.2 Electrochemical behaviour of PAni

Synthesis of PAni is accomplished by chemical polymerization which involves aniline oxidation by chemical oxidant ($K_2S_2O_8$) in an acidic medium. The polymerization reaction is carried out in an acidic medium to facilitate the protonation. The PAni H_2SO_4 has the original conductivity of 37 S cm^{-1}.[33] Drop-coating method was used as the deposition method of a thin PAni film on the substrate. The fabricated sensor was annealed at 100 °C for 1 hour as annealing increased the sensor's sensitivity by a factor of two.[6]

The general formula of PAni can be illustrated as in Fig. 6.[46,47] The emeraldine form of PAni is composed of reduced benzenoid units and oxidized quinoid units.[6,18] Both of these units have nitrogen atoms with a lone electron pair. Therefore, both can be protonated. Protonation of reduced form (eqn (1)) and

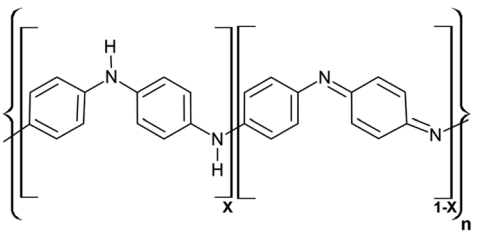

Fig. 6 General formula of PAni (where, $X = 1$; leucoemeraldine, $X = 0.5$; emeraldine and $X = 0$; pernigraniline as base forms).

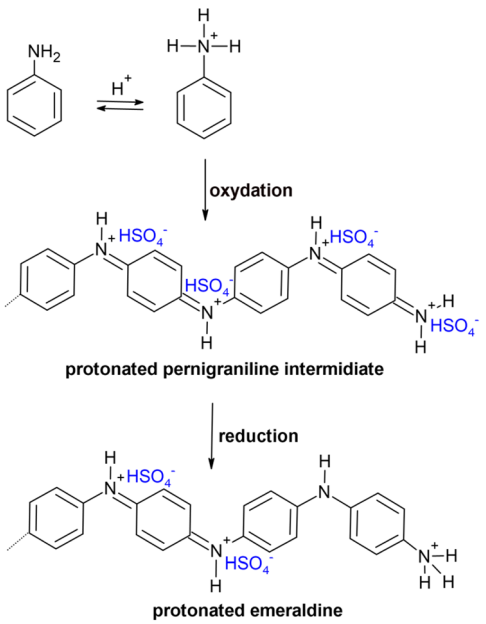

Fig. 7 Oxydation of aniline into emaraldine salt through pernigraniline intermediate in acidic medium.

protonation of oxidized form (eqn (2)) can be represented as follows, respectively.[6]

$$-NH- \rightarrow -NH_2^+- \quad (1)$$

$$-N= \rightarrow -NH^+= \quad (2)$$

These protonated sites, also known as charged sites or H-bond accepting/donating sites, contribute to the electrical conductivity of PAni.[8] Among three forms of PAni, protonated polyemaraldine or polyemaraldine salt is the conductive form which possesses conductivity around 15 S cm^{-1}.[48]

Fig. 7 shows the oxidation of aniline into polyemaraldine salt.[49] Oxidation in the presence of H_2SO_4 acid converts the aniline monomer into the anilinium cation. The growth of PAni chain takes place through the protonated pernigraniline intermediate. Following the consumption of the oxidant in the medium, the residual aniline reduces pernigraniline to the final product protonated emeraldine.[49] Chemical polymerization of aniline gives the green-colored product emeraldine salt. This form of PAni is more sensitive to water vapor. As the surface of PAni film is hydrophilic, it has high affinity to water vapour. The humidity sensitivity of PAni can be explained by two types of interactions that take place between water molecules and polymer. These are the formation of hydrogen bonds and swelling in conducting polymer.[48,50] Protons released from the water molecules interact with universally conjugated C=C double bonds. This phenomenon is used in humidity sensing.[51]

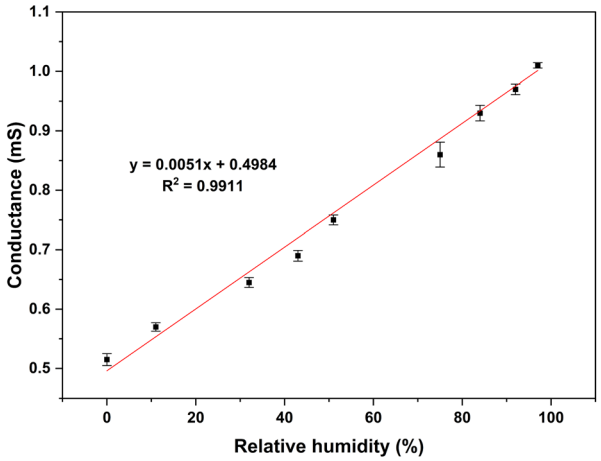

Fig. 8 Conductance *vs.* RH.

3.3 Humidity assisted conductivity of PAni

The enhanced charge transfer process facilitated by the water vapor increases the conductivity of PAni.[44] The absorbed moisture in PAni film causes the polymer swelling and consequently unfolding the polymer chain.[17] Since water molecules are ionisable, they can be dissociated into protons (H^+) and hydroxyl ions (OH^-). The charged sites on the PAni film facilitate the formation of proton through charge interactions and H-bonding. Accordingly, the absorbed water molecules serve as a proton source by increasing doping level and/or charge conducting.[23] Conductance variations obtained with different RH% are shown in Fig. 8. According to the results, conductance was increased with increasing humidity. The proposed sensor was capable of producing linear relationship between the humidity level and conductance.

The Fig. 9(i)–(v) show the steps in sensor fabrication process. As shown in Fig. 9(v) the humidity sensor consisted of a three-electrode system which included two graphite electrodes (working electrode and counter electrode) and a silver electrode (reference electrode). Here, the silver electrode was used as a pseudo reference electrode to control the potential.

The three-electrode configuration was used to achieve rapid response/recovery, high response and high precision.[52] The polymer part lying between the two carbon electrodes is crucial

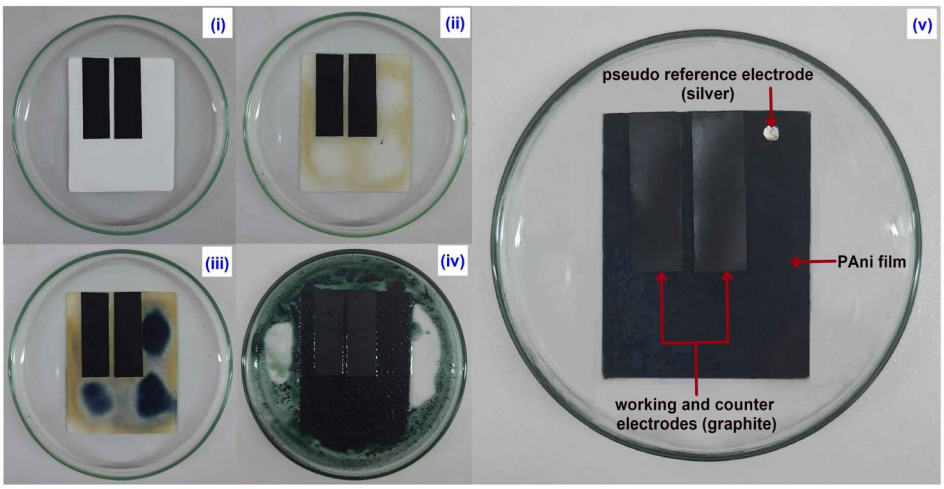

Fig. 9 Humidity sensor fabrication process: (i) fabricated graphite electrodes on chromatography paper substrate (ii) after a few moments of adding monomer and oxidant (iii) formation of blue coloured pernigraniline intermediate (iv) formation of green coloured emeraldine (v) finished fabricated PAni humidity sensor on paper with three-electrode configuration.

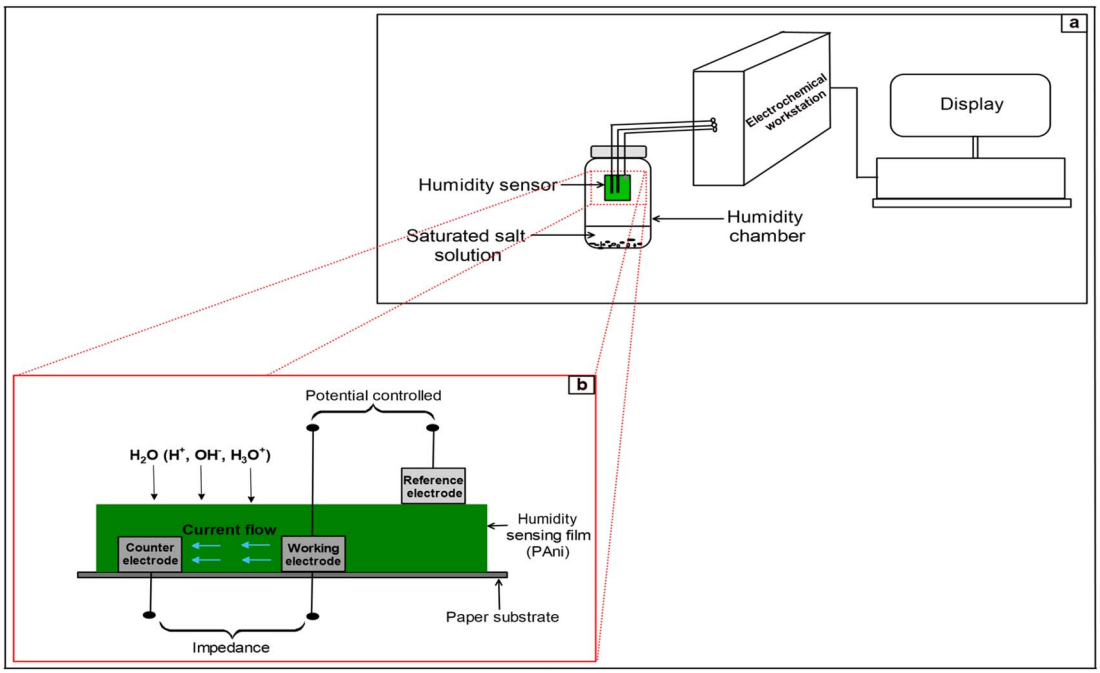

Fig. 10 Schematic diagram of (a) experimental setup of humidity sensor measuring system and (b) theoretical model of the sensor.

for the humidity response. Even though distance lowering between electrodes caused to decrease the film impedance, optimal distance between electrodes was selected in such a way that the impedance is not too high at low RH% and not too low at high RH%. This ensured clear impedance spectra over the entire frequency range.[53] Fig. 10(a) shows the experimental setup used to obtain Electrochemical impedance at different humidity levels and Fig. 10(b) shows the theoretical model of the sensor.

3.4 EIS response of humidity sensor

EIS was used to study the charge transport process in depth.[54] The electrochemical impedance spectra were collected using developed paper-based humidity sensor for the humidity series consisted of 0%, 11%, 32%, 43%, 51%, 75%, 84%, 92%, and 97% RH values. The Fig. 11 shows the Nyquist plots of the film at different humidity levels and can be used to describe the sensing mechanism of the humidity sensor.

Fig. 12 shows the response curves of the $|Z|$ *versus* RH% at different frequencies. The impedance increases monotonically with RH% at different frequencies. The linearity values of the fitted curves at different frequencies were closely similar with a $R^2 \approx 0.99$. However, high sensitivity/slope can be observed (increased rate is faster) at 1000 Hz. Therefore, 1000 Hz was selected as the most suitable frequency for further analysis.

Variation of highest $-Z''$, Z' at the point of intersection and $|Z|$ of the sensor against RH% are shown in Fig. 13(a)–(c) respectively. The $-Z''$, Z' and $|Z|$ values of the sensor showed negative correlation with RH%. The effect of humidity on impedance of the sensor can be easily clarified using sensitivity ($S_{z'}$, $S_{-z''}$ and $S_{|Z|}$) as given in the following eqn (3)–(5);

$$S_{z'} = \Delta Z'/\Delta \mathrm{RH} \quad (3)$$

$$S_{-z''} = \Delta -Z''/\Delta \mathrm{RH} \quad (4)$$

$$S_{|Z|} = \Delta |Z|/\Delta \mathrm{RH} \quad (5)$$

where $\Delta Z'$, $\Delta -Z''$, $\Delta |Z|$ and ΔRH are real impedance, negative imaginary impedance, impedance magnitude at 1000 Hz and RH increments, respectively.[55]

The sensitivity values can be obtained from the slope of the graphs plotted in Fig. 13(a)–(c). The sensitivity values for the sensor for the RH range of 0% to 97% were found to be $S_{z'} = -1.1623$ Ω/%RH, $S_{-z''} = -0.6495$ Ω/%RH and $S_{|Z|} = -1.1701$

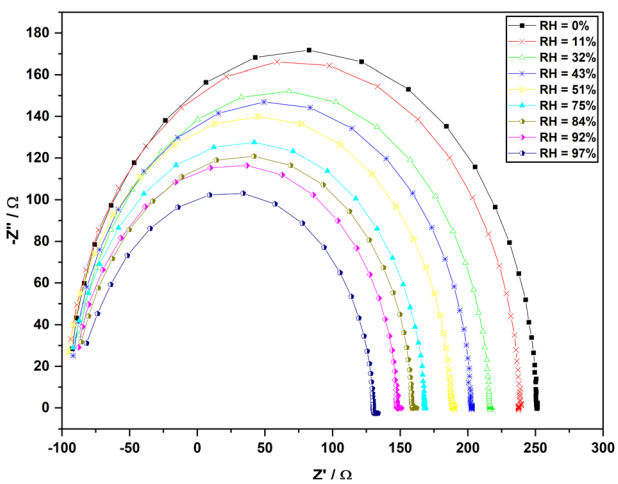

Fig. 11 Impedance spectra (negative imaginary impedance *vs.* real impedance) of the sensor at different humidity levels.

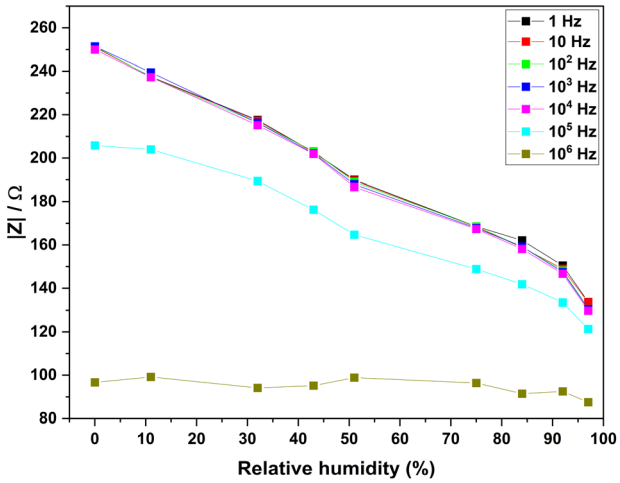

Fig. 12 $|Z|$ variation with humidity under different frequencies.

Ω/%RH. It can be seen from Fig. 13(a)–(c), the highest $-Z''$ *vs.* humidity, Z' *vs.* humidity and $|Z|$ *vs.* humidity produced linear plots with R^2 values of 0.9819, 0.9891 and 0.9900, respectively.

3.5 Humidity sensing mechanism

Electrical conductivity of PAni films arises due to H^+ ions from water and electrons.[56] The intrinsic impedance of the sensing film is the primary reason for the semicircle. With increasing RH, the intrinsic impedance of the sensing film decreases due to the interaction between the sensing film and water resulting in a decrease in the curvature of the semicircle.[57] As seen in Fig. 11, an obvious semi-circle can be seen in the spectrum of every humidity level in this developed sensor. This indicates that even at high humidity, the sensing process is not diffusion controlled. This may be due to the morphological features of PAni film limiting the diffusion process under high humidity and significant contribution from the electronic conduction.[58] However, as seen in Fig. 11, it can be observed a barely popped tail at the low-frequency region of Nyquist plots correspond to 84%, 92%, and 97% RH levels which is an indication of the Warburg impedance due to diffusion.

3.6 Effect of temperature on the impedance responses of humidity sensor

The temperature effect on the sensing mechanism was studied at different temperatures and Fig. 14 shows the experimental setup used. Two of impedance spectra were collected, one in a typical atmosphere at room temperature and other one in an N_2 gas flushed environment. The maximum value of $-Z''$ for the sensor in the N_2 gas flushed environment was found to be twenty times greater than in a normal atmosphere, and this trend was also observed for Z' values. This increase in impedance is attributed to the N_2 flushing which removes fixed water molecules from the PAni film.[59] As the temperature in the N_2 gas flushed environment increases, the film's impedance/resistance decreases, but remains higher compared to room temperature in a normal atmosphere. The relationship between the changes in impedance due to the N_2 flushing and the temperature-dependent behavior of PAni is depicted in Fig. 15. This

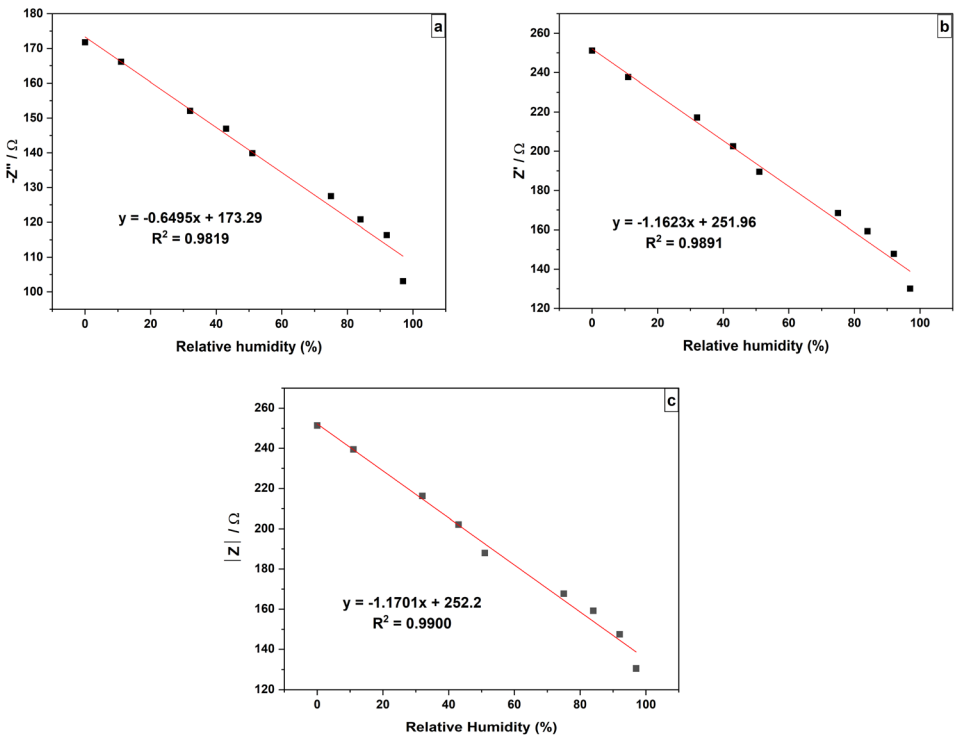

Fig. 13 Variation of (a) highest $-Z''$ values (b) Z' value at the intersection point of the impedance curve with the x-axis (c) $|Z|$ values at 1000 Hz frequency of the sensor for the RH% levels of 0%, 11%, 32%, 43%, 51%, 75%, 84%, 92% and 97%.

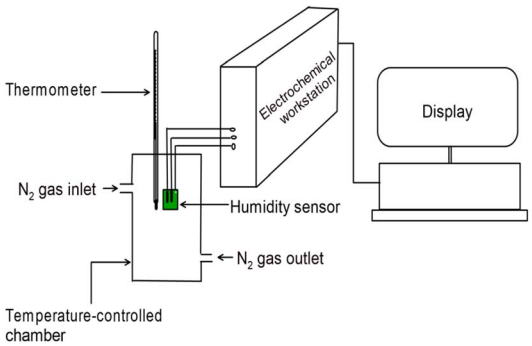

Fig. 14 Schematic diagram of experimental setup for studying the temperature effect.

decrease in resistance (an increase in conductivity) with increasing temperature strongly suggest the semiconducting behavior of PAni.[60] However, the electroactivity and conductivity of the PAni film were observed to be stable up to 135–140 °C.

High-temperature exposure reduced conductivity and electroactivity of PAni and temperatures above 150 °C resulted in irreversible conductivity loss. These changes may be associated with structural changes in the PAni film such as reactions of amine and imine groups reducing N atoms available for reprotonation.[61] With increasing temperature, the ionic conductivity due to H^+ hopping decreases and electronic conductivity increases. Charge transportation happens through thermally assisted hopping of electrons within the sites that are energetically close.[44]

3.7 Selectivity, stability and response/recovery study

The selectivity for humidity of the sensor is crucial in practical applications and it was studied analysing sensor responses for the ethanol vapor which can act as a polar interfering gas[62] and CO_2 which is a commonly available gas in atmosphere. According to the results shown in Fig. 16(a)–(i), there is no observable difference between complex impedance plots collected in the presence and absence of ethanol vapor at different humidity levels. As PAni has a high affinity with water vapor, it rapidly adsorbs water when in contact with a gas mixture containing water in the vapor phase.[15] Therefore, ethanol vapor has no significant effect on the sensor and can sense humidity without interference from ethanol vapor. According to the results obtained, there is no significant difference between two impedance spectra obtained in the presence and absence of CO_2 gas at every humidity level as can be clearly seen from the results shown in Fig. 17(a)–(i). Therefore, chemically polymerized PAni (emeraldine) shows no significant sensitivity toward CO_2 as water has high affinity to PAni matrix. However, the modified/improved PAni with a hydrophilic material such as PEDOT:PSS has been used to detect CO_2 as reported in previous studies.[63]

One of the most important parameters of a humidity sensor is its stability. The stability and the long-term RH sensing performance of the sensor was studied by comparing the impedance responses over a 30 day period under 11%, 75% and 97% RH conditions. As shown in Fig. 18(b), there was no significant impedance deviation was observed, indicating that the device has excellent stability.

The response reversibility of the sensor in different RH levels was further studied by taking reversible measurements by switching the sensor back and forth between RH 0% and continuously increasing RH levels in the 11–97% range. Fig. 18(d) shows the dynamic impedance response *versus* time plot with gradually increasing RH. It was observed that the impedance of the sensor immediately returns to its original state at different humidity levels demonstrating its good reversibility. Response time (t_{res}) and recovery time (t_{rec}) are crucial factors for the humidity sensor applications.[62,64] In this study, the response and recovery times are defined as the time

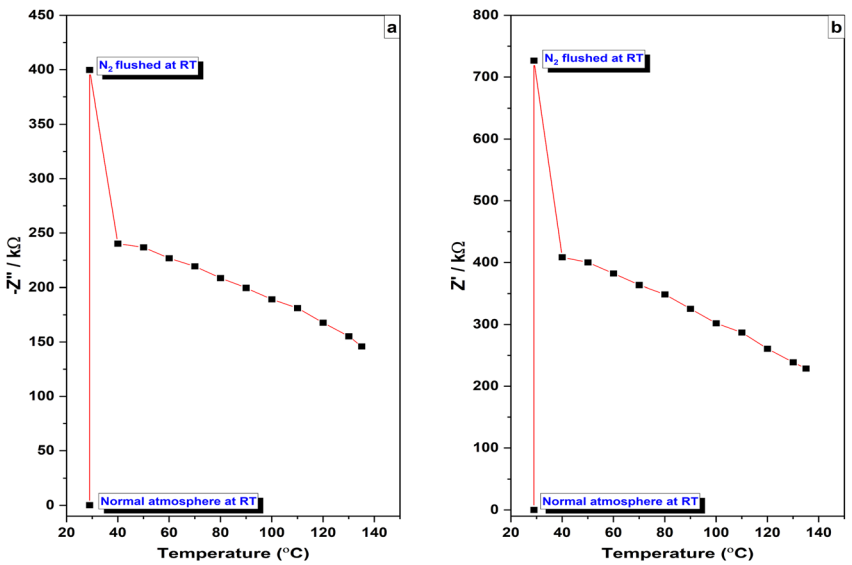

Fig. 15 Variation of (a) highest $-Z''$ values and (b) Z' values at the intersection with the x-axis with temperature.

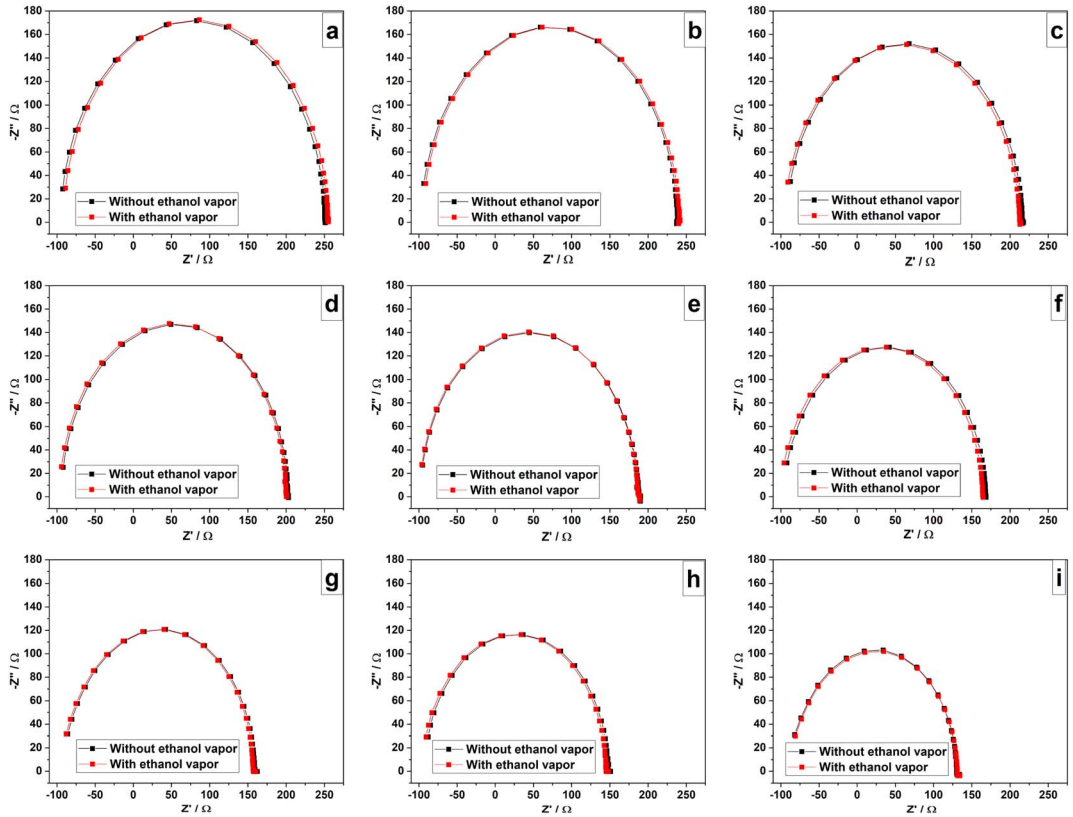

Fig. 16 Complex impedance plots of the sensor at RH levels of (a) 0% (b) 11% (c) 32% (d) 43% (e) 51% (f) 75% (g) 84% (h) 92% (i) 97% with and without ethanol vapor.

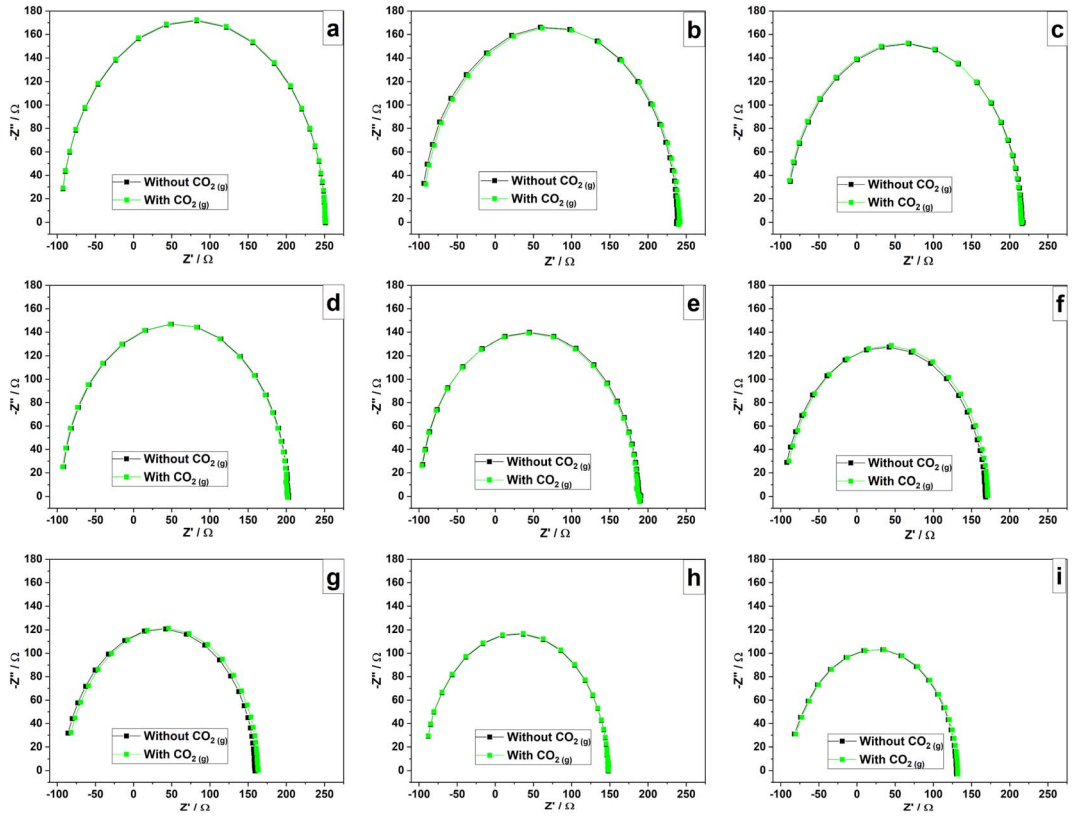

Fig. 17 Complex impedance plots of the sensor at RH levels of (a) 0% (b) 11% (c) 32% (d) 43% (e) 51% (f) 75% (g) 84% (h) 92% (i) 97% with and without CO_2 gas.

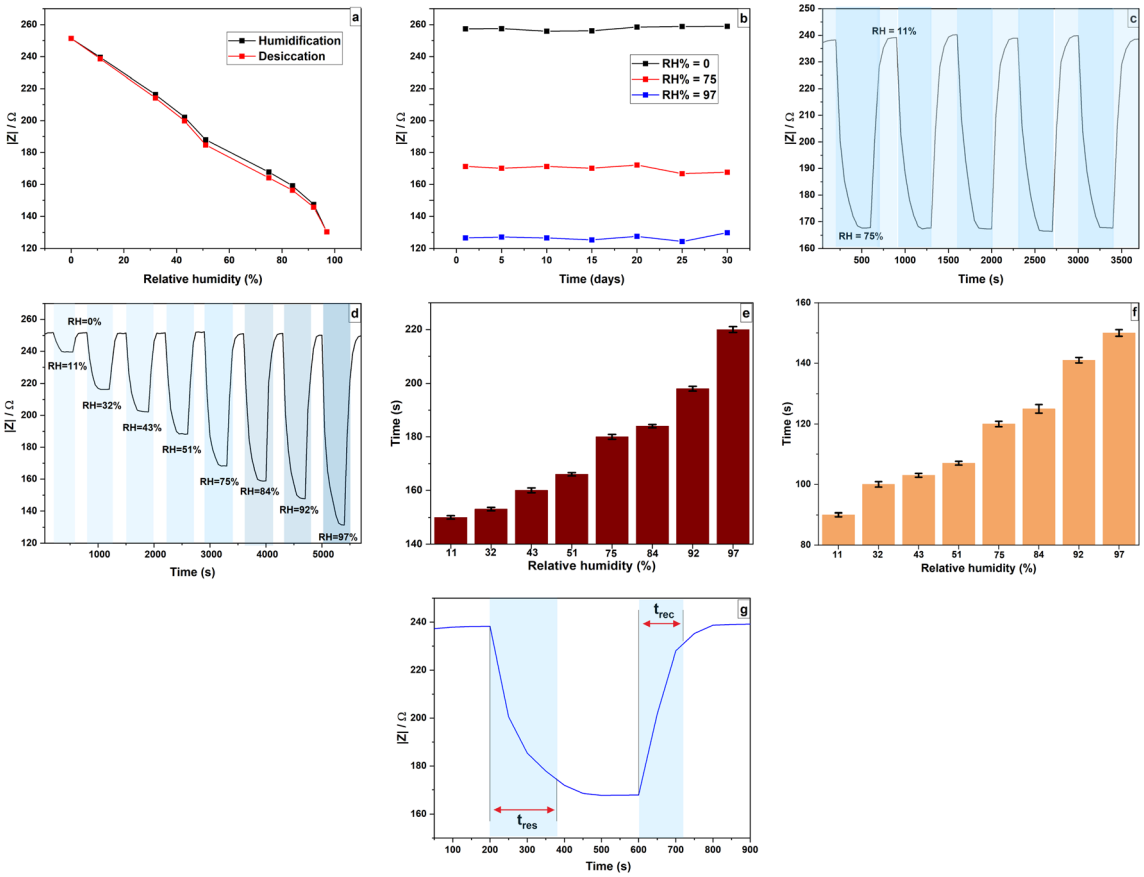

Fig. 18 Humidity sensing properties of the sensor (a) long-term stability, (b) hysteresis of the sensor, (c) repeatability curves of the sensor for humidity level variations from 11% to 75%, (d) dynamic impedance response curves with gradually increasing humidity. Summary of variation of (e) response time, (f) recovery time in different RH environments. (g) The dynamic response–recovery curve of the sensor for 11% and 75% RH levels.

the sensor takes to reach 90% of the equilibrium point when exposed to different RH environments.[65] The t_{res} and t_{rec} values at a given fixed humidity point were measured and recorded. As shown in Fig. 18(e) and (f), the response and recovery time of the sensor increase as humidity increases. The response time of the sensor ranged from 150 to 220 s in a wide humidity range and the maximum recovery time observed was 150 s, which corresponds to the highest RH level, 97%. The repeatability of the sensor was studied by switching the sensor between 11% and 75% RH levels for five successive cycles and responses were recorded with an average response time of 180 s and an average recovery time of 120 s. Fig. 18(c) shows the repeatability of the sensor and Fig. 18(g) shows the response–recovery time curve of the sensor for switching between 11% and 75%. The standard deviation values of measured responses at 11% and 75% RH levels are as low as 0.132 and 0.054, respectively. In addition, the standard deviations of response and recovery time to switch the sensor between 11% and 75% RH levels are as low as 2.24 and 1.20, respectively. The response curves are almost identical at a given humidity indicating good repeatability with a fast response–recovery behaviour.

The hysteresis can be used to determine the reliability of the sensor and it is shown in the Fig. 18(a). The impedance measurements were collected for the absorption process (from 0% RH to 97% RH) and desorption process (from 97% RH to 0% RH) in cyclic way. It can be seen that impedance values for the entire humidification process is always greater than for the desiccation process. The sensor exhibited maximum hysteresis of about 2.1% at 75% RH level. This low hysteresis value accounts for the rapid adsorption and desorption rate of water molecules on the PAni surface.[66] The hysteresis depends on the film thickness. A thin film results in low hysteresis as differences in the rates of absorption and desorption are low.[8]

The substrates of chemical sensors have an important influence on sensing performance.[67] The strong interaction between PAni and cellulose in the paper occur due to hydrogen bonds that exist between the hydroxyl groups of glucose and the repeating N-functionality in PAni, which can affect the sensing behavior of PAni.[68] This is evident from the differences in the linearity (R^2) of the impedance responses of the paper-based humidity sensor ($R^2 = 0.9900$) and the identical sensor on a PET substrate ($R^2 = 0.8702$), as shown in Fig. 13 and S4 (in ESI†), respectively.

Table 1 compares humidity sensors developed using PAni and PAni based compounds. Typically, humidity sensor development requires the utilization of expensive chemicals and costly fabrication procedures. Kundu *et al.* reported PAni-encased multiwall carbon nanotubes for humidity sensing

Table 1 Comparison of PAni based humidity sensors developed with different substrates and fabrication methods

Sensing material	Substrate	Fabrication method	Sensing principle	Detection range (%RH)	Response (%)	Linear response behaviour (R^2)	Selectivity	Mechanical status	Electrode system	Max. hysteresis (%)	t_{res}/t_{rec} (s)	Ref.
CNT/PAni	PET	*In situ* polymerization	Resistance	10–90	42.6	0.992	—	Flexible	Two silver electrodes	2.68	23/120	69
PAni/SLS	Paper	*In situ* polymerization	Resistance	5–95	99.2	0.99	Tested against different pressure conditions	Flexible	Interdigitated silver electrodes	1.5	18/35	75
PAni	Glass	LBL nano-assembly	Resistance	50–90	23	—	—	Rigid	Silver contact electrodes	—	15/27	73
Cell/PAni	Cellulose fiber	*In situ* polymerization	Current	2–50	13	0.999	—	Flexible	2 Extremities link to the potentiostat	—	370/1490 (long cycling)	68
PAni	Glass	Chemical Polymerization	Impedance	10–95	28	—	—	Rigid	—	3.89	—	76
PAni	Glass	Drop-casting	Impedance	36–90	—	—	—	Rigid	Two electrodes (Au and Ag)	2.0	8/27	6
Nanogranular PAni	Paper	*In situ* polymerization	Resistance	16–96.2	90.29	≈0.996	Against SO_2, CO_2, CH_4, H_2	Flexible	—	6.8	1300/2809	71
PAni	Paper	Ink jet printing	Impedance	16–98	200	—	—	—	PEDOT: PSS electrodes	—	10 min/—	72
PAni	Glass	Rapid mixing polymerization	Resistance	11.5–56 ppm	≈12	(CF) 0.917	—	Rigid	—	—	520/30	44
PAni/TiO_2	Glass	Spin coating	Impedance	25–95	84.21	—	—	Rigid	Interdigitated silver electrodes	—	60/100	77
PAni nanofibers	—	Drop coating	Resistance	0–95	88	—	—	—	Two Screen-printed carbon electrodes	—	—	23
PAni pellet	—	*In situ* polymerization	Resistance	20–95	20	—	—	—	—	—	5/10	78
PAni	Paper	Drop coating	Impedance	0–97	48	0.990	Tested against ethanol$_{(g)}$ and $CO_{2(g)}$	Flexible	Three-electrode configuration	2.1	220/150	This work

which involves complex time-intensive process that demands advanced techniques, involves high-temperature conditions and requires specialized equipment.[69] Therefore, low cost is significant in humidity sensor development as it facilitates wider access to the technology, drives mass adoption, provides cost-effective solutions, and allows easy integration into a variety of devices and systems. Some fabrication techniques have limitations. For example, Chethan *et al.* developed PAni/WGO composites and utilized *in situ* polymerization method which has limitations such as impracticability to bulk production of the composites and resulting poor interconnecting network among polymer chains and fillers.[70] Sandhu *et al.* reported a nanogranular PAni-integrated paper as a humidity sensor with better responsivity. However, it was noted to have a drawback of having a lengthy response and recovery time, taking 1300 s and 2809 s respectively.[71] The PAni/PEDOT: PSS humidity sensor developed by Morais *et al.* has the same problem of long response time.[72] Ragazzini *et al.* proposed a humidity sensor developed with conductive paper sheets produced using PAni and cellulose. The RH% detection range was narrow and limited to low RH levels, from 2–50 RH% while response and recovery times are comparatively high.[68] Su *et al.* reported a disposable humidity sensor based on ultrathin PAni film. The layer-by-layer nano-assembly method was used as polymer deposition method to improve sensing performance *via* changing polymer molecular structure. However, the RH% detection range of this sensor was narrow and limited to high RH levels.[73] Many humidity sensing parameters are interdependent.[74] Therefore, at designing phase, based on the target application, several criteria must be taken into account to determine which parameters should be prioritized over others.[74]

4. Conclusions

In this study, the humidity sensing properties of PAni were studied using the EIS technique. The results have clearly shown, that increasing RH decreases the film impedance. This dependence of impedance on the humidity of the developed paper-based PAni sensor makes it suitable for use in humidity meters. The sensor exhibits high sensitivity and good linearity in the range of 0 to 97% RH, as well as fast response and recovery times, low hysteresis, long-term stability and good repeatability. The characterization of the PAni film of the sensor using different techniques revealed the presence of the emaraldine salt form and films are highly porous. Additionally, the results indicated that the substrate has an impact on the sensor's sensing mechanism and sensitivity, and paper was found to be a better option compared to polyester. It was also found that there is an effect of the temperature on the conduction mechanism of the sensor where impedance decreases with increasing temperature. Furthermore, obtained results show that ethanol vapor and CO_2 gas have no observable effect on the sensor. Therefore, this sensor can be used to sense humidity without interference from CO_2 and ethanol vapor. The sensor possesses unique features that maximize the humidity sensing, making it a promising candidate in environmental monitoring, research activities, medical and industrial applications, *etc* as a flexible, low-cost and disposable humidity sensor with easy fabrication steps.

Conflicts of interest

There are no conflicts to declare.

Acknowledgements

The authors gratefully acknowledge the Centre for Analytical Research and Development (CARD) and Centre for Advanced Materials and Devices (CAMD) at Department of Chemistry, University of Colombo for providing laboratory support to this study and Mr G. D. D. S. Gamage of University of Peradeniya, Sri Lanka, for his support on Scanning Electron Microscopy.

Notes and references

1 Y. Feng, S. Wang, B. Feng, R. Wang, Y. He and T. Zhang, Development of an auto test system for humidity sensors, *Sens. Actuators, A*, 2009, **152**, 104–109, DOI: 10.1016/j.sna.2009.03.001.
2 P. G. Su and P. H. Lu, Electrical and humidity-sensing properties of impedance-type humidity sensors that were made of ag microwires/ppy/sno2 ternary composites, *Chemosensors*, 2020, **8**(4), 1–14, DOI: 10.3390/chemosensors8040092.
3 H. Farahani, R. Wagiran and H. M. Nizar, Humidity Sensors Principle, Mechanism, and Fabrication Technologies, *Sensors*, 2014, **14**, 7881–7939, DOI: 10.3390/s140507881.
4 B. Adhikari and S. Majumdar, *Polymers in sensor applications*, 2004, **29**, 699–766, DOI: 10.1016/j.progpolymsci.2004.03.002.
5 S. Diab, Y. Bashan, Y. Okon and Y. Henis, Effects of relative humidity on Bacterial Scab Caused by Xanthomonas campestris pv. vesicatoria on Pepper, *Phytopathology*, 1982, **72**, 1257–1260, DOI: 10.1094/Phyto-72-1257.
6 M. T. S. Chani, K. S. Karimov, F. A. Khalid and S. A. Moiz, Polyaniline based impedance humidity sensors, *Solid State Sci.*, 2013, **18**, 78–82, DOI: 10.1016/j.solidstatesciences.2013.01.005.
7 A. V. Arundel, E. M. Sterling, J. H. Biggin and T. D. Sterling, Indirect health effects of relative humidity in indoor environments, *Environ. Health Perspect.*, 1986, **65**(3), 351–361, DOI: 10.1289/ehp.8665351.
8 M. T. S. Chani, K. S. Karimov, F. A. Khalid, S. Z. Abbas and M. B. Bhatty, Orange dye - Polyaniline composite based impedance humidity sensors, *Chin. Phys. B*, 2013, **22**(1), 010701, DOI: 10.1088/1674-1056/22/1/010701.
9 R. Gupta, J. A. Fereiro, A. Bayat, A. Pritam, M. Zharnikov and P. C. Mondal, Nanoscale molecular rectifiers, *Nat. Rev. Chem.*, 2023, **7**, 106–122, DOI: 10.1038/s41570-022-00457-8.
10 H. Bai and G. Shi, Gas Sensors Based on Conducting Polymers, *Sensors*, 2007, **7**, 267–307, DOI: 10.3390/s7030267.
11 S. Liang, X. He, F. Wang, *et al.*, Sensors and Actuators B : Chemical Highly sensitive humidity sensors based on LiCl – Pebax 2533 composite nanofibers via electrospinning,

Sens. Actuators, B, 2015, **208**, 363–368, DOI: 10.1016/j.snb.2014.11.035.

12 M. Gereadr, A. Choubey and B. Malhotra, Review: Application of Conducting Polymer to Biosensors, *Biosens. Bioelectron.*, 2001, **17**, 345–359.

13 T. Riaz, F. Kanwal, S. A. Siddiqi, N. Gull and T. Jamil, Study of Conducting Properties of Chemically Synthesized Polyaniline/crystalline Silica Composites, *Int. J. Sci. Eng. Res.*, 2016, **7**(6), 513–519.

14 K. M. Ziadan, Conducting Polymers Application, *New Polym. Spec. Appl.*, 2012, 3–24, DOI: 10.5772/48316.

15 J. Fraden, *Handbook of Modern Sensors, Physics, Design and Applications*, 3rd edn, 2003.

16 M. A. Shishov and I. Y. Sapurina, *Oxidative polymerization of Aniline: molecular synthesis of polyaniline and the formation of supramolecular structures*, 2012, DOI: 10.5772/48758.

17 A. G. Mustafin, L. R. Latypova, A. N. Andriianova, *et al.*, Polymerization of new aniline derivatives: synthesis, characterization and application as sensors, *RSC Adv.*, 2021, **11**(34), 21006–21016, DOI: 10.1039/d1ra02474d.

18 K. M. Molapo, P. M. Ndangili, R. F. Ajayi, *et al.*, Electronics of conjugated polymers (I): polyaniline, *Int. J. Electrochem. Sci.*, 2012, **7**(12), 11859–11875, DOI: 10.1016/j.solidstatesciences.2013.01.005.

19 D. J. Walton, Electrically conducting polymers, *Mater. Des.*, 1990, **11**(3), 142–152, DOI: 10.1016/0261-3069(90)90004-4.

20 N. Gospodinova and L. Terlemezyan, Conducting polymers prepared by oxidative polymerization: polyaniline, *Prog. Polym. Sci.*, 1998, **23**(8), 1443–1484, DOI: 10.1016/S0079-6700(98)00008-2.

21 K. Deb, A. Bera, K. L. Bhowmik and B. Saha, Conductive polyaniline on paper as a flexible electronic material with controlled physical properties through vapor phase polymerization, *Polym. Eng. Sci.*, 2018, **58**(12), 2249–2255, DOI: 10.1002/pen.24845.

22 M. V. Kulkarni, S. K. Apte, S. D. Naik, J. D. Ambekar and B. B. Kale, Ink-jet printed conducting polyaniline based flexible humidity sensor, *Sens. Actuators, B*, 2013, **178**, 140–143, DOI: 10.1016/j.snb.2012.12.046.

23 F. W. Zeng, X. X. Liu, D. Diamond and K. T. Lau, Humidity sensors based on polyaniline nanofibres, *Sens. Actuators, B*, 2010, **143**(2), 530–534, DOI: 10.1016/j.snb.2009.09.050.

24 S. Manjunatha, B. Chethan, Y. T. Ravikiran and T. Machappa. Room Temperature Humidity Sensor Based on Polyaniline-Tungsten Disulfide Composite. 2018030096. DOI: 10.1063/1.5032431.

25 H. S. Kim, J. H. Kang, J. Y. Hwang and U. S. Shin, Wearable CNTs-based humidity sensors with high sensitivity and flexibility for real-time multiple respiratory monitoring, *Nano Convergence*, 2022, **9**(1), 35, DOI: 10.1186/s40580-022-00326-6.

26 L. Greenspan, Humidity fixed points of binary saturated aqueous solutions, *J. Res. Natl. Bur. Stand., Sect. A*, 1977, **81A**(1), 89, DOI: 10.6028/jres.081A.011.

27 D. P. Dissanayake, H. M. P. C. K. Herath, E. K. C. Pradeep, M. K. Jayananda, J. K. D. S. Jayanetti and V. Kapaklis, Glass surface functionalized with polyaniline as a fast responding humidity sensor, *Sens. Transducers J.*, 2012, **137**(2), 137–144.

28 ASTM International E104-02, *Standard practice for maintaining constant relative humidity by means of aqueous solutions*, ASTM Stand, 2003, vol. E104-85, pp. 32–34, 0652R.

29 I. Must, U. Johanson, F. Kaasik, I. Poldsalu, A. Punning and A. Aabloo, An ionic liquid-based actuator as a humidity sensor, *2013 IEEE/ASME Int Conf Adv Intell Mechatronics Mechatronics Hum Wellbeing, AIM*, 2013, vol. 2013, pp. 1498–1503, DOI: 10.1109/AIM.2013.6584307.

30 S. Gul, A. U. H. A. Shah and S. Bilal, Synthesis and characterization of processable polyaniline salts, *J. Phys.: Conf. Ser.*, 2013, **439**(1), DOI: 10.1088/1742-6596/439/1/012002.

31 P. Y. Wong, S. W. Phang and A. Baharum, Effects of synthesised polyaniline (PAni) contents on the anti-static properties of PAni-based polylactic acid (PLA) films, *RSC Adv.*, 2020, **10**(65), 39693–39699, DOI: 10.1039/d0ra07076a.

32 M. Trchová, Z. Morávková, I. Šeděnková and J. Stejskal, Spectroscopy of thin polyaniline films deposited during chemical oxidation of aniline, *Chem. Pap.*, 2012, **66**(5), 415–445, DOI: 10.2478/s11696-012-0142-6.

33 M. Trchová, I. Šeděnková, E. Tobolková and J. Stejskal, FTIR spectroscopic and conductivity study of the thermal degradation of polyaniline films, *Polym. Degrad. Stab.*, 2004, **86**(1), 179–185, DOI: 10.1016/j.polymdegradstab.2004.04.011.

34 A. Quayoum, Humidity Sensor Using Polyaniline-Metal Oxide Composites, *J. Adv. Res. Sci. Soc. Sci.*, 2004, **3**(1), 9–15.

35 B. Butoi, A. Groza, P. Dinca, A. Balan and V. Barna, Morphological and structural analysis of polyaniline and poly(o-anisidine) layers generated in a DC glow discharge plasma by using an oblique angle electrode deposition configuration, *Polymers*, 2017, **9**(12), 732, DOI: 10.3390/polym9120732.

36 S. Palaniappan, C. Saravanan, C. A. Amarnath and V. J. Rao, Polyaniline Salts and Complexes as Catalyst in Bisindole Synthesis, *Catal. Lett.*, 2004, **97**, 77–81, DOI: 10.1023/B:CATL.0000034291.79388.19.

37 I. Šed, M. Trchová and J. Stejskal, The Influence of Acidity on Polymerization of Aniline: Interpretation of Large Number of Spectra Using Factor Analysis, *WDS'06 Proc. Contrib. Papers, Part III – Phys.*, 2006, 70–75.

38 M. N. Costa, B. Veigas and J. M. Jacob, A low cost, safe, disposable, rapid and self-sustainable paper-based platform for diagnostic testing: lab-on-paper, *Nanotechnology*, 2014, **25**(9), 094006, DOI: 10.1088/0957-4484/25/9/094006.

39 M. Alice, C. Mazzeu and L. K. Faria, Structural and Morphological Characteristics of Polyaniline Synthesized in Pilot Scale, *J. Aerosp. Technol. Manage.*, 2017, **9**, 39–47, DOI: 10.5028/jatm.v9i1.726.

40 G. Firpo, E. Angeli, P. Guida, S. R. Lo, L. Repetto and U. Valbusa, Gas permeation through rubbery polymer nano-corrugated membranes, *Sci. Rep.*, 2018, **8**(1), 1–10, DOI: 10.1038/s41598-018-24551-4.

41 C. C. Buron, B. Lakard, A. F. Monnin, V. Moutarlier and S. Lakard, Elaboration and characterization of polyaniline films electrodeposited on tin oxides, *Synth. Met.*, 2011, **161**(19–20), 2162–2169, DOI: 10.1016/j.synthmet.2011.08.021.

42 M. J. Giz, S. L. De Albuquerque Maranhão and R. M. Torresi, AFM morphological study of electropolymerised polyaniline films modified by surfactant and large anions, *Electrochem. Commun.*, 2000, **2**(6), 377–381, DOI: 10.1016/S1388-2481(00)00041-2.

43 C. Steffens, A. Manzoli, F. L. Leite, O. Fatibello and P. S. P. Herrmann, Atomic force microscope microcantilevers used as sensors for monitoring humidity, *Microelectron. Eng.*, 2014, **113**, 80–85, DOI: 10.1016/j.mee.2013.07.015.

44 M. Joulazadeh, A. H. Navarchian and M. Niroomand, A comparative study on humidity sensing performances of polyaniline and polypyrrole nanostructures, *Adv. Polym. Technol.*, 2014, **33**(S1), 1–10, DOI: 10.1002/adv.21461.

45 H. Xu, J. Gao, M. Li, *et al.*, Mesoporous WO 3 nanofibers with crystalline framework for high-performance acetone sensing, *Front. Chem.*, 2019, **7**, 1–11, DOI: 10.3389/fchem.2019.00266.

46 K. I. Ajeel and Q. S. Kareem, Synthesis and Characteristics of Polyaniline (PANI) Filled by Graphene (PANI/GR) nano-Films, *J. Phys.: Conf. Ser.*, 2019, **1234**(1), 012020, DOI: 10.1088/1742-6596/1234/1/012020.

47 N. Haddar, A. Kallel, J. F. Pilard and P. Daniel, Synthesis and investigation of flexible conductive nanocomposite polyurethanes/polyaniline doped with NICL2, *Polym. Bull.*, 2022, **79**(4), 2523–2538, DOI: 10.1007/s00289-021-03647-4.

48 D. Nicolas-Debarnot and F. Poncin-Epaillard, Polyaniline as a new sensitive layer for gas sensors, *Anal. Chim. Acta*, 2003, **475**(1–2), 1–15, DOI: 10.1016/S0003-2670(02)01229-1.

49 J. Stejskal, I. Sapurina, M. Trchová and E. N. Konyushenko, Oxidation of aniline: polyaniline granules, nanotubes, and oligoaniline microspheres, *Macromolecules*, 2008, **41**(10), 3530–3536, DOI: 10.1021/ma702601q.

50 G. E. Collins and L. J. Buckley, Conductive polymer-coated fabrics for chemical sensing, *Synth. Met.*, 1996, **78**(2), 93–101, DOI: 10.1016/0379-6779(96)80108-1.

51 Z. Chen and C. Lu, *Humidity Sensors : A Review of Materials and Mechanisms*, 2005, **3**(2), 274–295, DOI: 10.1166/sl.2005.045.

52 Z. Shi, M. Pan, J. Liu and J. Sheng, Design and detection method of three-electrode humidity sensor based on micro-arc MgO, *Appl. Phys. A: Mater. Sci. Process.*, 2021, **127**(7), 1–11, DOI: 10.1007/s00339-021-04662-y.

53 M. J. Yang, Y. Li, N. Camaioni, G. Casalbore-Miceli, A. Martelli and G. Ridolfi, Polymer electrolytes as humidity sensors: progress in improving an impedance device, *Sens. Actuators, B*, 2002, **86**(2–3), 229–234, DOI: 10.1016/S0925-4005(02)00190-9.

54 P. Jash, R. K. Parashar, C. Fontanesi and P. C. Mondal, The Importance of Electrical Impedance Spectroscopy and Equivalent Circuit Analysis on Nanoscale Molecular Electronic Devices, *Adv. Funct. Mater.*, 2021, **32**(10), 2109956, DOI: 10.1002/adfm.202109956.

55 A. Din, K. S. Karimov, K. Akhtar, *et al.*, Impedimetric humidity sensor based on the use of SnO_2–Co_3O_4 spheres, *J. Mater. Sci.: Mater. Electron.*, 2017, **28**(5), 4260–4266, DOI: 10.1007/s10854-016-6049-1.

56 T. C. D. Doan, R. Ramaneti, J. Baggerman, H. D. Tong, A. T. M. Marcelis and C. J. M. Van Rijn, Intrinsic and ionic conduction in humidity-sensitive sulfonated polyaniline, *Electrochim. Acta*, 2014, **127**, 106–114, DOI: 10.1016/j.electacta.2014.01.150.

57 H. Bi, K. Yin and X. Xie, Ultrahigh humidity sensitivity of graphene oxide, *Sci. Rep.*, 2013, **3**, 2714, DOI: 10.1038/srep02714.

58 Y. Li, B. Ying, L. Hong and M. Yang, Water-soluble polyaniline and its composite with poly(vinyl alcohol) for humidity sensing, *Synth. Met.*, 2010, **160**(5–6), 455–461, DOI: 10.1016/j.synthmet.2009.11.031.

59 A. Alix, V. Lemoine, M. Nechtschein, J. P. Travers and C. Menardo, Water absorption study in polyaniline, *Synth. Met.*, 1989, **29**(1), 457–462, DOI: 10.1016/0379-6779(89)90333-0.

60 I. Bekri-Abbes and E. Srasra, Electrical and dielectric properties of polyaniline and polyaniline/montmorillonite nanocomposite prepared by solid reaction using spectroscopy impedance, *J. Nanomater.*, 2015, **2015**, 516902, DOI: 10.1155/2015/516902.

61 R. Ansari, W. E. Price and G. G. Wallace, Effect of thermal treatment on the electroactivity of polyaniline, *Polymer*, 1996, **37**(6), 917–923, DOI: 10.1016/0032-3861(96)87273-9.

62 Z. Wu, J. Yang, X. Sun, *et al.*, An excellent impedance-type humidity sensor based on halide perovskite $CsPbBr_3$ nanoparticles for human respiration monitoring, *Sens. Actuators, B*, 2021, **337**, 129772, DOI: 10.1016/j.snb.2021.129772.

63 L. C. ting, *A Room Temperature Operated Carbon Dioxide Sensor Based on EB-PANI/PEDOT, PSS Sensing Material*, 2016, pp. 23–26.

64 C. Zhang, Y. Zhang, K. Cao, *et al.*, Ultrasensitive and reversible room-temperature resistive humidity sensor based on layered two-dimensional titanium carbide, *Ceram. Int.*, 2021, **47**(5), 6463–6469, DOI: 10.1016/j.ceramint.2020.10.229.

65 N. Kaur, M. Singh and E. Comini, One-Dimensional Nanostructured Oxide Chemoresistive Sensors, *Langmuir*, 2020, **36**(23), 6326–6344, DOI: 10.1021/acs.langmuir.0c00701.

66 A. Tripathy, S. Pramanik, A. Manna, *et al.*, Design and development for capacitive humidity sensor applications of lead-free Ca, Mg, Fe, Ti-oxides-based electro-ceramics with improved sensing properties via physisorption, *Sensors*, 2016, **16**(7), 1135, DOI: 10.3390/s16071135.

67 J. Wu, Z. Wu, K. Tao, *et al.*, Rapid-response, reversible and flexible humidity sensing platform using a hydrophobic and porous substrate, *J. Mater. Chem. B*, 2019, **7**(12), 2063–2073, DOI: 10.1039/c8tb02963f.

68 I. Ragazzini, R. Castagnoli, I. Gualandi, *et al.*, A resistive sensor for humidity detection based on cellulose/polyaniline, *RSC Adv.*, 2022, **12**(43), 28217–28226, DOI: 10.1039/d2ra03982f.

69 S. Kundu, R. Majumder, R. Ghosh, *et al.*, Relative humidity sensing properties of doped polyaniline-encased multiwall carbon nanotubes: wearable and flexible human respiration monitoring application, *J. Mater. Sci.*, 2020, **55**(9), 3884–3901, DOI: 10.1007/s10853-019-04276-z.

70 B. Chethan, H. G. Raj Prakash, Y. T. Ravikiran, *et al.*, Enhancing humidity sensing performance of polyaniline/water soluble graphene oxide composite, *Talanta*, 2019, **196**, 337–344, DOI: 10.1016/j.talanta.2018.12.072.

71 S. S. Sandhu, S. Kumar, S. Augustine, *et al.*, Nanoengineered conductive polyaniline enabled sensor for sensitive humidity detection, *IEEE Sens. J.*, 2020, **20**(21), 12574–12581, DOI: 10.1109/JSEN.2020.3001599.

72 R. M. Morais, M. D. S. Klem, G. L. Nogueira, T. C. Gomes and N. Alves, Low Cost Humidity Sensor Based on PANI/PEDOT:PSS Printed on Paper, *IEEE Sens. J.*, 2018, **18**(7), 2647–2651, DOI: 10.1109/JSEN.2018.2803018.

73 R. Nohria, R. K. Khillan, Y. Su, R. Dikshit, Y. Lvov and K. Varahramyan, Humidity sensor based on ultrathin polyaniline film deposited using layer-by-layer nano-assembly, *Sens. Actuators, B*, 2006, **114**(1), 218–222, DOI: 10.1016/j.snb.2005.04.034.

74 M. Sajid, Z. J. Khattak, K. Rahman, G. Hassan and K. H. Choi, Progress and future of relative humidity sensors: a review from materials perspective, *Bull. Mater. Sci.*, 2022, **45**(4), 238, DOI: 10.1007/s12034-022-02799-x.

75 J. Mahlknecht, G. Wuzella, H. Lammer and M. Khalifa, A smart functional surfactant activated conductive polymer coated on paper with ultra-sensitive humidity sensing characteristics, *Mater. Adv.*, 2022, **3**(3), 1804–1815, DOI: 10.1039/d1ma00740h.

76 R. Kumar and B. C. Yadav, Humidity sensing investigation on nanostructured polyaniline synthesized via chemical polymerization method, *Mater. Lett.*, 2016, **167**, 300–302, DOI: 10.1016/j.matlet.2016.01.082.

77 S. Kotresh, Y. T. Ravikiran, H. G. R. Prakash and S. C. V. Kumari, Polyaniline-Titanium dioxide composite as humidity sensor at room temperature, *Nanosyst.: Phys., Chem., Math.*, 2016, 732–739, DOI: 10.17586/2220-8054-2016-7-4-732-739.

78 S. Jain, S. Chakane, A. B. Samui, V. N. Krishnamurthy and S. V. Bhoraskar, Humidity sensing with weak acid-doped polyaniline and its composites, *Sens. Actuators, B*, 2003, **96**(1–2), 124–129, DOI: 10.1016/S0925-4005(03)00511-2.